Dalton Transactions

Benzyne addition to a metal-carbon multiple bond

Harrison J. Barnett and Anthony F. Hill*

Received 19th April 2021,
Accepted 00th January 20xx

DOI: 10.1039/x0xx00000x

www.rsc.org/

Experimental Procedures

Unless otherwise stated, experimental work was carried out at room temperature under a dry and oxygen-free nitrogen atmosphere using standard Schlenk techniques with dried and degassed solvents.

NMR spectra were obtained on a Bruker 400 (^{1}H at 400.1 MHz, ^{13}C at 100.6 MHz, ^{31}P at 162.0 MHz), a Bruker Avance 600 (^{1}H at 600.0 MHz, ^{13}C at 150.9 MHz) or a Bruker Avance 700 (^{1}H at 700.0 MHz, ^{13}C at 176.1 MHz) spectrometers at the temperatures indicated. Chemical shifts (δ) are reported in ppm with coupling constants given in Hz and are referenced to the solvent peak, or external references (H_3PO_4 in H_2O for ^{31}P). Multiplicities given in parentheses (^{31}P) are from NMR simulations performed in gNMR. The multiplicities of NMR resonances are denoted by the abbreviations s (singlet), d (doublet), t (triplet), m (multiplet), br (broad) and combinations thereof for more highly coupled systems. In some cases, distinct peaks were observed in the ^{1}H and ^{13}C{^{1}H} NMR spectra, but to the level of accuracy that is reportable (i.e. 2 decimal places for ^{1}H NMR, 1 decimal place for ^{13}C NMR) they are reported as having the same chemical shift. The abbreviation 'dppm C_6H_5' is used to refer to the phenyl rings on the (diphenylphosphino)methane ligand. Spectra provided generally correspond to samples obtained directly from chromatography and may contain residual solvent as recrystallised samples often display reduced solubility.

Infrared spectra were obtained using a PerkinElmer FTIR spectrometer. The strengths of IR absorptions are denoted by the abbreviations vs (very strong), s (strong), m (medium), w (weak), sh (shoulder) and br (broad). Elemental microanalytical data were provided by Macquarie University. High-resolution electrospray ionisation mass spectrometry (ESI-MS) was performed by the ANU Research School of Chemistry mass spectrometry service with acetonitrile as the matrix.

[a] *Research School of Chemistry, Australian National University, Canberra, Australian Capital Territory, ACT 2601, Australia.*
†Corresponding author: Email: a.hill@anu.edu.au
Electronic Supplementary Information (ESI) available: Synthetic procedures, spectroscopic and crystallographic data. See DOI: 10.1039/x0xx00000x. CCDC 2035999 and 2069151 contain the supplementary crystallographic data for this paper. These data can be obtained free of charge from The Cambridge Crystallographic Data Centre.

Data for X-ray crystallography were collected with an Agilent SuperNova CCD diffractometer using Cu-Kα radiation (λ = 1.54184 Å) at 150 K using the CrysAlis PRO software.[1] The structures were solved iteratively (intrinsic phasing) using the SHELXT program and refined by full-matrix least-squares on F^2 using the SHELXL program.[2] Hydrogen atoms were located geometrically and refined using a riding model. Diagrams were produced using the CCDC visualisation program Mercury.[3]

The synthesis of **1** has been described previously.[4] All other chemicals were purchased and used as described. 'TBAF' refers to a commercially available (Sigma-Aldrich product 216143) 1.0 M solution in THF purported to contain 5% wt% (ca 3 M) water.

Synthesis of $[Rh_2(\mu_2\text{-}C)(\mu\text{-}Cl)(\kappa_2\text{-}C_6H_4)(C_6H_5)Cl_2(\mu\text{-dppm})_2]$ (2). To a flask containing **1** (0.050 g, 0.047 mmol)

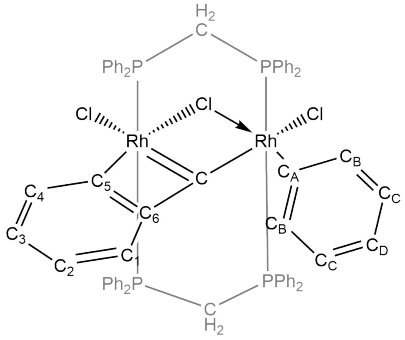

and 2-(trimethylsilyl)phenyl trifluoromethanesulfonate (0.023 mL, 1.229 gcm^{-3}, 0.095 mmol) was added acetonitrile (20 mL). To this red solution, TBAF (1.0 M solution in THF, 0.10 mL, 0.10 mmol) was added, and the resulting dark red solution was stirred for two hours. After this time the volatiles were removed *in vacuo* and the residue was subjected to column chromatography (10 x 1 cm silica gel column), eluting initially with neat CH_2Cl_2 and then with 1:19 THF:CH_2Cl_2. An orange/pink band was collected, and the volatiles were removed under reduced pressure to give a pink microcrystalline solid of pure **2** (0.019 g, 0.015 mmol, 32%). IR (ATR, cm^{-1}): 3050w, 2935w, 1434s. ^{1}H NMR (400 MHz, $CDCl_3$, 298 K): δ_H = 2.78 (s, 4H, PCH_2P), 5.36 (d, J = 7.3 Hz, 1H, H_1), 6.00 (dd, J = 7.4 Hz, 2H, H_C), 6.22 (t, J= 7.1 Hz, 1H, H_D), 6.60 (dd, J = 7.6 Hz, 1H, H_3), 6.74 (dd, J = 7.4 Hz, 1H, H_2), 6.77 (d, J = 7.7 Hz, 2H, H_B), 6.95 (t, J = 7.7 Hz, 4H, dppm C_6H_5), 7.00-7.02 (m, 9H, dppm C_6H_5), 7.06-7.13 (m, 12H, dppm C_6H_5),

7.20-7.23 (m, 6H, dppm C_6H_5), 7.37-7.40 (m, 4H, dppm C_6H_5), 7.60 (d, J = 7.8 Hz, 1H, H_4), 7.88-7.91 (m, 4H, dppm C_6H_5), 8.23-8.25 (m, 4H, dppm C_6H_5).
$^{13}C\{^1H\}$ NMR (151 MHz, $CDCl_3$, 298 K): δ_C = 394.8 (m, μ_2-C), 171.3 (m, C_5), 144.9 (dt, $^1J_{RhC}$ = 35 Hz, $^2J_{RhP}$ = 7 Hz, C_A), 141.6 (s, C_B), 138.7-139.0 (m, C_6), 138.1 (s, C_2), 136.5, 136.2 (2 x m, dppm C_6H_5), 135.8 (s, C_1), 133.9, 133.4 (2x m, dppm C_6H_5 *ipso*), 131.8 (s, dppm C_6H_5), 130.8 (m, dppm C_6H_5), 130.5 (s, dppm C_6H_5), 129.8 (s, dppm C_6H_5), 129.5 (s, dppm C_6H_5), 128.0 (m, dppm C_6H_5), 127.8 (m, dppm C_6H_5), 127.5 (m, dppm C_6H_5), 127.1 (t, J = 25 Hz, dppm C_6H_5), 124.5 (s, C_C), 124.2 (s, C_3), 121.7 (s, C_D), 120.7 (s, C_4), 22.9-23.0 (m, -CH_2-). $^{31}P\{^1H\}$ NMR (162 MHz, $CDCl_3$, 298 K): δ_P = 1.93 (ddd, $^1J_{RhP}$ = 119 Hz, $^3J_{RhP}$ = (21) Hz, $^4J_{PP}$ = (11) Hz), 6.92 (ddd, $^1J_{RhP}$ = 125 Hz, $^3J_{RhP}$ = (21) Hz, $^4J_{PP}$ = (11) Hz). MS (ESI, *m/z*): Found: 1209.0574. Calcd for $C_{57}H_{50}{}^{35}Cl_2P_4{}^{103}Rh_2$ $[M–Cl]^+$: 1209.0585. Anal. Found: C, 59.89; H, 4.74%. Calcd for $C_{63}H_{53}Cl_3P_4Rh_2$: C, 59.95; H, 4.37%. Crystals suitable for structure determination were grown by slow evaporation of a CH_2Cl_2/toluene mixture. *Crystal data for* $C_{63}H_{53}Cl_3P_4Rh_2.C_7H_8$: ($M_w$ = 1328.16 g.mol^{-1}): tetragonal, space group $P4_12_12$, a = 15.01727(5), c = 26.39108(12) Å, V = 5951.67(5) Å^3, Z = 4, T = 150.0(1) K, pink block 0.11 x 0.095 x 0.045, μ(CuKα) = 7.03 mm^{-1}, D_{calc} = 1.391 Mg.m^{-3}, 108169 reflections measured (8.2° ≤ 2Θ ≤ 147.2°), 6006 unique (R_{int} = 0.034) which were used in all calculations. The final R_1 was 0.030 ($I > 2\sigma(I)$) and wR_2 was 0.082 (all data) for 472 refined parameters with 334 restraints. CCDC 2035999. An orthorhombic space group refinement of this dataset was used to confirm the approximately 50:50 disorder of the benzyne/phenyl ligands.

The synthesis of the isotopologue **[Rh$_2$(μ$_2$-^{13}C)(μ-Cl)(κ$_2$-C$_6$H$_4$)(C$_6$H$_5$)Cl$_2$(μ-dppm)$_2$]** (**2'**) was achieved through identical reaction conditions when using **[Rh$_2$(μ$_2$-^{13}C)Cl$_2$(μ-dppm)$_2$]** as the starting material.

Synthesis of [Rh$_2$(μ-CC$_6$H$_4$)(μ-Cl)RCl$_2$(μ-dppm)$_2$] (R = Cl, C$_6$H$_5$ 1:1 admixture). To a flask containing [Rh$_2$(μ$_2$-C)Cl$_2$(μ-dppm)$_2$] (0.033 g, 0.031 mmol), ammonium chloride (0.055 g, 1.03 mmol, 33 eq.), and 2-(trimethylsilyl)phenyl trifluoromethanesulfonate (0.050 mL, 0.206 mmol) was added acetonitrile (25 mL). To this yellow solution was added TBAT (0.039 g, 0.072 mmol). The solution remains yellow in colour and is stirred for 15 hours at room temperature. After this time, the volatiles were removed *in vacuo* and the residue was subjected to column chromatography (10 x 1 cm silica gel column), eluting initially with neat CH_2Cl_2 and then with 1:19 THF:CH_2Cl_2. A yellow band was collected, and the volatiles were removed under reduced pressure to give a beige inseparable mixture of **2** and **4** in equal amounts (combined yield 0.012 g). IR (ATR, cm^{-1}): 3052, 3050, 2937, 1434. ^{1}H NMR (400 MHz, $CDCl_3$, 298 K): δH = 2.74, 3.01 (2 x m, 4H, -PCH_2P), 5.23 (d, J = 7.4 Hz, 1H, H_1), 6.73 (dd, J = 7.3 Hz, 1H, H_3), 6.84 (dd, J = 7.4 Hz, 1H, H_2), 6.95 (t, J = 7.7 Hz, 4H, dppm C_6H_5), 7.42-7.53 (m, 12H, dppm C_6H_5), 7.62-7.65 (m, 3H, dppm C_6H_5), 7.68-7.73 (m, 4H, dppm C_6H_5), 8.03 (d, J = 7.8 Hz, 1H, H_4), 8.06-8.11 (m, 4H, dppm C_6H_5). Remaining aromatic environments were unable to be clearly distinguished from those of **2**. The ^{13}C NMR data was unable to be distinguished from that of **2** . $^{31}P\{^1H\}$ NMR (162 MHz, CDCl3, 298 K): δ_P = 0.74 (dt, $^1J_{RhP}$ = 96 Hz, $^3J_{RhP}$ = 14 Hz), 7.14 (m). MS (ESI, *m/z*): Found: 1167.0416. Calcd for $C_{57}H_{48}{}^{35}Cl_3P_4{}^{103}Rh_2$ $[M–Cl]+$: 1166.9882. Anal. Found: C, 59.90; H, 4.75%. Calcd for 0.5($C_{63}H_{53}Cl_3P_4Rh_2$) + 0.5($C_{57}H_{48}Cl_4P_4Rh_2$): C, 60.57; H, 4.28%. A crystal suitable for structure determination was grown by slow evaporation of a CH_2Cl_2/toluene mixture. Crystal data for $C_{60}H_{50.5}Cl_{3.5}P_4Rh_2$ (0.5 **2** + 0.5 **4**) (M = 1225.28 g.mol^{-1}): tetragonal, space group $P4_12_12$, a = 14.9951(1), c = 26.1521(4) Å, V = 5880.38(12) Å^3, Z = 4, T = 150.0(1) K, μ(CuKα) = 7.31 mm^{-1}, Dcalc = 1.384 g.cm^{-3}, 10253 reflections measured (4.2° ≤ 2Θ ≤ 141.6°), 5538 unique (R_{int} = 0.028) which were used in all calculations. The final R_1 was 0.034 (I > 2σ(I)) and wR_2 was 0.100 (all data) for 365 refined parameters with 97 restraints. CCDC 2069151.

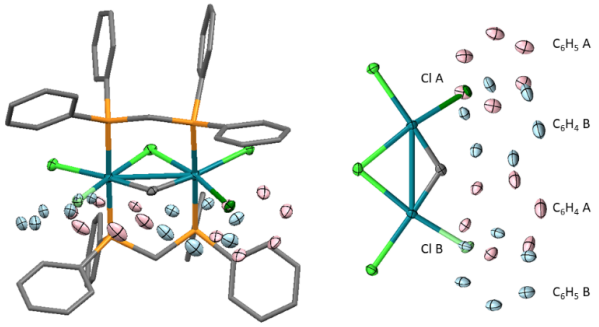

Figure S1. Superimposed molecular structures of [Rh$_2$(μ-CC$_6$H$_4$)(μ-Cl)RCl$_2$(μ-dppm)$_2$] (R = Cl **4**, C$_6$H$_5$ **2**) in a crystal of **4$_{0.5}$.2$_{0.5}$**. Inset: symmetry-driven dual-occpuancy of benzyne and phenyl ligands (in pink and blue) and further 1:1 occupation of chloride ligand (light and dark green).

Author Contributions

Both HJB and AFH contributed equally to the conceptualization, experimental design, interpretation of experimental results and manuscript compilation. All experimental procedures and data acquisition, including structural analysis, were executed by HJB. AFH was responsible for overall project administration and direction.

Computational Details

Computational studies were performed by using the *SPARTAN18*® suite of programs.[4] Geometry optimisation (gas phase) was performed at the DFT level of theory using the exchange functional (ωBP97X-D) of Head-Gordon.[5] The Los Alamos effective core potential type basis set (LANL2Dζ) of Hay

and Wadt[6] was used for Rh; the Pople 6-31G* basis sets[7] were used for all other atoms. Frequency calculations were performed to confirm that the optimized structures were minima and also to identify vibrational modes of interest.

$[Rh_2(\mu\text{-}CC_6H_4)HCl_2(\mu\text{-}dHpm)_2]$

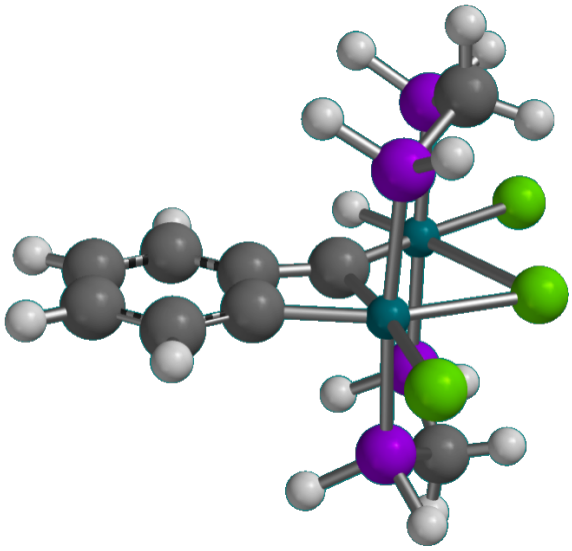

Figure S2. Optimised geometry for $[Rh_2(\mu\text{-}CC_6H_4)HCl_2(\mu\text{-}dHpm)_2]$ (DFT:ωBP97X-D/LANL2Dζ, gas phase).

Cartesian Coordinates

Atom	x	y	z
Rh1	-0.711963251	0.126857496	-1.307713837
Cl2	1.527358830	-0.257983134	-2.561218844
Rh3	2.153453700	-0.381621426	0.135408908
C4	0.279552300	-0.049903988	0.353357211
C5	-0.812579126	0.140570405	1.266953177
C6	-3.347271782	0.584004419	2.174158857
C7	-1.863967872	0.326074431	0.340547732
C8	-1.003242273	0.172736525	2.654231191
C9	-2.299692003	0.399636331	3.094442708
C10	-3.155626561	0.551875499	0.788861888
H11	-0.176989281	0.027862482	3.344944763
H12	-2.516890044	0.436775005	4.157175138
H13	-3.983326195	0.697824180	0.102238582
H14	-4.348040226	0.758292942	2.561882362
Cl15	-2.254314271	0.403545975	-3.241153890
Cl16	4.527007885	-0.798882154	-0.253898929
P17	-1.013611237	-2.190933871	-1.357971236
P18	1.717794347	-2.667102826	0.080892468
P19	-0.205785451	2.409329728	-1.349319159
P20	2.522427255	1.917747534	0.096022588
Atom	**x**	**y**	**z**
C21	1.602004578	2.813992443	-1.238717752
H22	1.754221606	3.893374779	-1.152518350
H23	2.038999755	2.465209257	-2.179911575
C24	0.550148585	-3.183570413	-1.259743796
H25	1.079201459	-2.984702554	-2.197660864
H26	0.330490158	-4.252568372	-1.191163669
H27	2.356564007	-0.424212121	1.654625127
H28	2.819114303	-3.505252634	-0.141479065
H29	1.154183182	-3.276254881	1.217742019
H30	-1.801448477	-2.783529511	-0.351490303
H31	-1.618086015	-2.718025471	-2.507646782
H32	-0.588132339	3.109499971	-2.501871254
H33	-0.753206047	3.232858099	-0.345818507
H34	3.843357313	2.333473721	-0.122533604
H35	2.198293189	2.673002135	1.238346697

Thermodynamic properties (298.15 K): *ZPE* = 587.50 kJmol^{-1}, H^o = –3317.833482 au, S^o = 720.02 Jmol^{-1}K^{-1}, G^o = –3317.915247, C_v = 383.59 Jmol^{-1}K^{-1}.

$[Rh_2(\mu\text{-}CC_6H_4)(C_6H_5)Cl_2(\mu\text{-}dmpm)_2]$

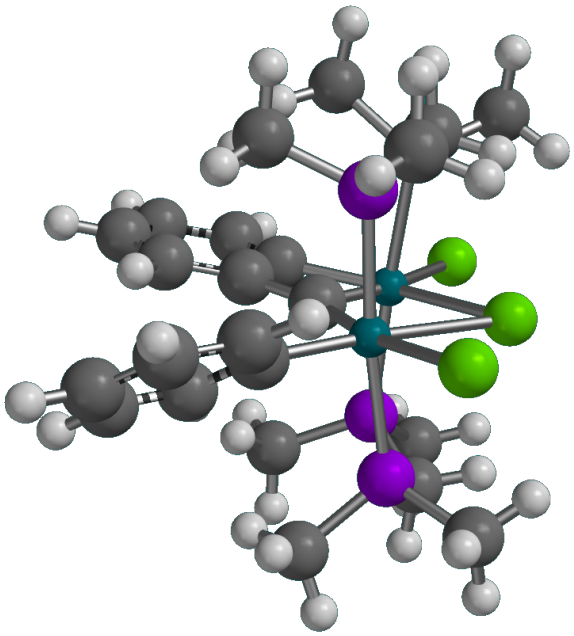

Figure S3. Optimised geometry for $[Rh_2(\mu\text{-}CC_6H_4)(C_6H_5)Cl_2(\mu\text{-}dmpm)_2]$ (DFT:ωBP97X-D/LANL2Dζ, gas phase).

Cartesian Coordinates

Atom	x	y	z
Rh1	1.342018490	-0.223594627	-1.705344106
Cl2	-0.903698993	0.064796810	-2.965051705
Rh3	-1.512925520	0.240693025	-0.262146754
C4	0.361031776	-0.076687439	-0.043051414
C5	1.466960916	-0.396082618	0.852221019
C6	4.013085010	-1.054470236	1.648537032
C7	2.499478713	-0.521704215	-0.103194484
C8	1.687781359	-0.630288305	2.217116872
C9	2.982884745	-0.962127989	2.597868336
C10	3.791069277	-0.843602729	0.285143253
H11	0.886205229	-0.564989020	2.945478702
Atom	**x**	**y**	**z**
H12	3.205356429	-1.153201241	3.643209857
H13	4.591732086	-0.946004613	-0.441079706
H14	5.013201940	-1.311187385	1.989928932
C15	-1.878601870	0.507102321	1.713518669
C16	-2.433394323	0.848570543	4.467679961
C17	-0.968734237	1.136161069	2.569186574
C18	-3.089361432	0.072940740	2.269914081
C19	-3.358731008	0.235966496	3.627700187
C20	-1.237680726	1.307264774	3.927305167
H21	-0.022364511	1.500788245	2.183373265
H22	-3.848143433	-0.356036847	1.625033332
H23	-4.309663217	-0.109735026	4.024849868

H24	-0.503770643	1.800861627	4.559664469
H25	-2.647007996	0.977704225	5.524625350
Cl26	2.991080091	-0.486182909	-3.598447965
Cl27	-3.927687106	0.395543670	-0.890419494
P28	1.701584104	2.094483268	-1.617391541
P29	-1.299613510	2.576939314	-0.717045721
P30	0.848151929	-2.532581002	-1.855839964
P31	-1.733225478	-2.099534987	-0.050260875
C32	-0.906214816	-2.966044554	-1.448345849
H33	-1.000248333	-4.051517112	-1.318940367
H34	-1.483698182	-2.674174363	-2.333032047
C35	0.122380571	3.018478512	-1.818842762
H36	-0.214107846	2.785587725	-2.834584081
H37	0.305487424	4.098379599	-1.755197588
C38	2.755458812	2.804873717	-2.922297444
H39	3.753174775	2.367634417	-2.840583979
H40	2.805997403	3.895435750	-2.839599532
H41	2.356415245	2.508537011	-3.894931464
C42	2.418665503	2.752530486	-0.065360861
H43	3.424788055	2.342654254	0.060130190
H44	1.823780830	2.430062052	0.793535868
H45	2.470298836	3.845586830	-0.085059420
C46	-1.136649013	3.751559845	0.681045423
H47	-0.193323778	3.608036480	1.211848624
H48	-1.951768876	3.575358737	1.387408329
H49	-1.186683798	4.781505622	0.313556846
C50	-2.688761965	3.282066810	-1.664844508
H51	-2.465014454	4.317020936	-1.945077331
H52	-3.597346982	3.236603692	-1.061962792
H53	-2.850760894	2.668500548	-2.553473655
C54	1.857318855	-3.645917389	-0.811060646
H55	2.896901582	-3.556814902	-1.139304371
H56	1.535467878	-4.687827326	-0.904298461
H57	1.811870967	-3.337879499	0.236865740
C58	-1.048745520	-2.853358337	1.468756113
H59	0.013413853	-2.621652723	1.565934353
H60	-1.187149696	-3.938982181	1.462613817
H61	-1.569720471	-2.423149731	2.328972417
C62	-3.419269872	-2.791209871	-0.129236860
H63	-3.377208952	-3.885410504	-0.131840866
H64	-3.917126502	-2.417285321	-1.025624443
H65	-3.992215988	-2.450287738	0.735976800
C66	1.005584083	-3.228400206	-3.532033518
H67	2.040635329	-3.111691317	-3.859405060
H68	0.376976969	-2.639718324	-4.204897619
H69	0.704380876	-4.280896564	-3.549890196

Thermodynamic properties (298.15 K): *ZPE* = 1377.33 kJmol^{-1}, H^o = –3863.047647 au, S^o = 1033.44 Jmol^{-1}K^{-1}, G^o = –3863.165004, C_v = 673.71 Jmol^{-1}K^{-1}.

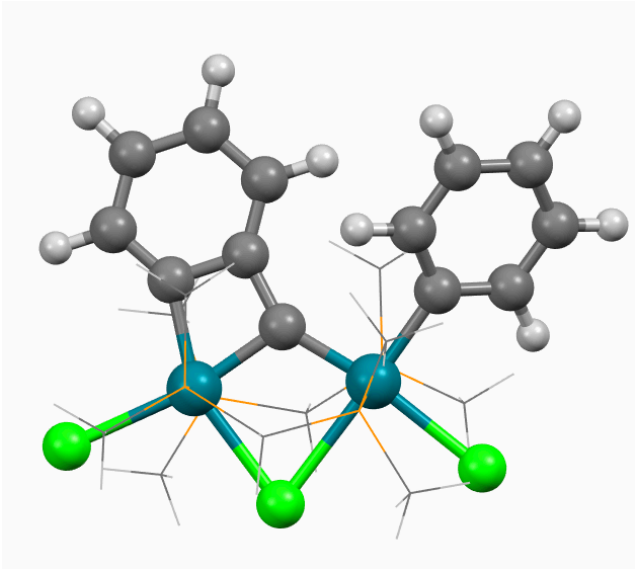

Figure S4. View of molecular geometry perpendicular to the equatorial coordination plane of optimised geometry for [Rh_2(μ-CC_6H_4)(C_6H_5)Cl_2(μ-dmpm)$_2$] (DFT:ωBP97X-D/LANL2Dζ, gas phase) with dmpm ligands simplified.

Mechanistic Conjecture

From the outset it should be noted that the following mechanistic conjecture, whilst plausible, has yet to be substantiated. Nevertheless, some observations are noteworthy in allowing us to exclude some potential pathways.

The formation of **2** involves both rhodium centres being oxidised from Rh^I to Rh^{III}. Whilst oxidation of the first is a result of the benzyne cyclo-addition, the oxidation of the second which involves installation of a σ-phenyl ligand remains obscure. Scheme S1 presents what we believe to a possible route by which **2** might arise.

According to the original Kobayashi protocol,[8] fluoride results in desilylation of 2-$Me_3SiC_6H_4OTf$ via an intermediate fluorosilicate $[FMe_3SiC_6H_4OTf]^-$ [9]. Departure of the fluorosilane $FSiMe_3$ is considered to be rapidly followed by dissociation of the triflate to generate benzyne, such that the 2-triflatophenyl anion does not accumulate sufficiently to be protonated by adventitious water. We may therefore presume that both benzyne and phenyltriflate are potentially available when an excess of the TBAF/$Me_3SiC_6H_4OTf$ reagent is employed.

Formation of the cyclometallated benzylidyne ligand is consistent with the formal cycloaddition of benzyne across one Rh=C bond however the intimate details of how this occurs are not clear. Three alternative routes seem plausible. Firstly, a simple [2+2] cyclo-addition would mimic the behaviour of benzyne with other unsaturated reagents.

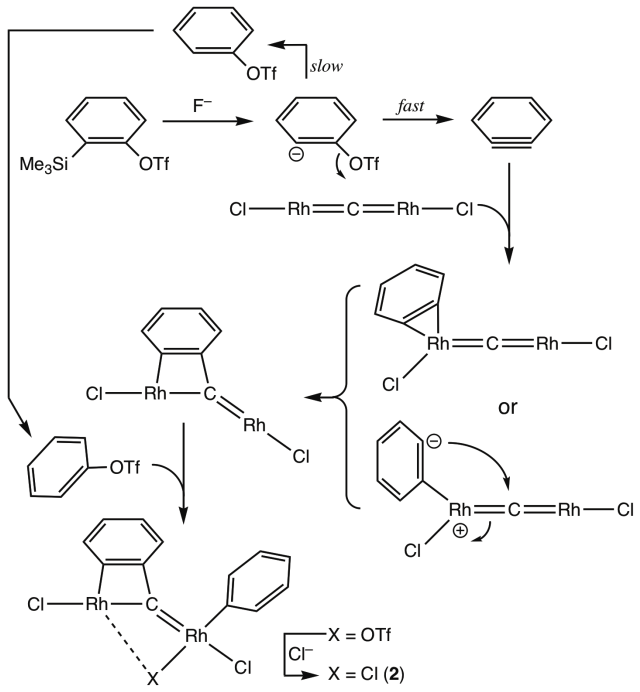

Scheme S1. Mechanistic proposal for the formation of **2**. Only equatorial ligand sets shown, μ-dppm ligands omitted.

The presence of rhodium, however raises the possibility that the metal might play a more significant role. Although benzyne complexes have not previously been prepared via actual addition of benzyne (or $Me_3SiC_6H_4OTf$) to an unsaturated metal centre, this is not unreasonable. Coordination of the benzyne *cis* to the Rh=C could then be followed by coupling in a manner completely analogous to alkyne or ene-yne metathesis. Finally, a two-step dipolar process might be envisaged in which a zwitterionic 2-rhodaphenyl carbanion collapses by nucleophilic attack at the bridging carbido ligand.

The second benzyne mode of installation in the form of a σ-phenyl ligand remains equivocal however the following observations are germane, suggesting that slow hydrolysis of $Me_3SiC_6H_4OTf$ to afford PhOTf may provide the source of the σ-phenyl ligand.

i) The rhodium carbido complex **1** does not react with $Me_3SiC_6H_4OTf$ until fluoride is added, i.e., oxidative addition to provide an intermediate 2-silyphenyl ligand may be excluded as the first step.

ii) This does not preclude the possible oxidative addition of PhOTf (from gradual hydrolysis of $[FMe_3SiC_6H_4OTf]^-$) or $Me_3SiC_6H_4OTf$ to the remaining rhodium(I) centre ONCE carbido-benzyne coupling has occurred.

iii) Conversion of coordinate triflate to chloride presumably occurs via scrambling.

iv) Complex **1** is unreactive towards the combination of fluoride and trimethylsilanes devoid of triflato substitutents, e.g., $PhSiMe_3$/TBAT.

v) The $^{31}P\{^1H\}$ spectra of crude **2** and **4** do not change upon chromatography (CH_2Cl_2, silica gel).

vi) Addition of excess chloride ($[^nBu_4N]Cl$) does not increase the yield of **2** indicating that the low yield is not a corollary of requisite halide scrambling.

References

1 Agilent, Agilent Technologies Ltd, Yarnton, Oxfordshire, England, 2014.

2 (a) G. Sheldrick, *Acta Crystallogr. Sect. A: Found. Crystallogr.* 2008, **64**, 112-122; (b) G. M. Sheldrick, *Acta Crystallogr. Sect. C: Cryst. Struct. Commun.* 2015, **71**, 3-8.

3 (a) C. F. Macrae, P. R. Edgington, P. McCabe, E. Pidcock, G. P. Shields, R. Taylor, M. Towler, J. van de Streek, *J. Appl. Crystallogr.* 2006, **39**, 453-457; (b) C. F. Macrae, I. J. Bruno, J. A. Chisholm, P. R. Edgington, P. McCabe, E. Pidcock, L. Rodriguez-Monge, R. Taylor, J. van de Streek, P. A. Wood, *J. Appl. Crystallogr.* 2008, **41**, 466-470.

4 H. J. Barnett and A. F. Hill, *Chem. Commun.*, 2019, **55**, 1734-1737.

5 *Spartan 18*® (2018) Wavefunction, Inc., 18401 Von Karman Ave., Suite 370 Irvine, CA 92612 U.S.A

6 J.-D. Chai and M. Head-Gordon, *J. Chem. Phys.*, 2008, **128**, 0841061–18410615; (*b*) J.-D. Chai and M. Head-Gordon, *Phys. Chem. Chem. Phys.*, 2008, **10**, 6615– 6620.

7 (a) P. J. Hay and W.R. Wadt, *J. Chem. Phys.*, 1985, **82**, 270-283. (b) W. R. Wadt and P. J. Hay, *J. Chem. Phys.* 1985, **82**, 284-298. (c) P. J. Hay, W. R. Wadt, *J. Chem. Phys.,* 1985, **82**, 299-310.

8 W. J. Hehre, R. Ditchfeld and J. A. Pople, *J. Chem. Phys.*, 1972, **56**, 2257-2261.

9 Y. Himeshima, T. Sonada and H. Kobayashi, *Chem. Lett.,* 1983, 1211-1214.

10 S. Liu, Y. Li and Y. Lan, *Eur. J. Org. Chem.* **2017**, 6349-6353.

Dalton Transactions

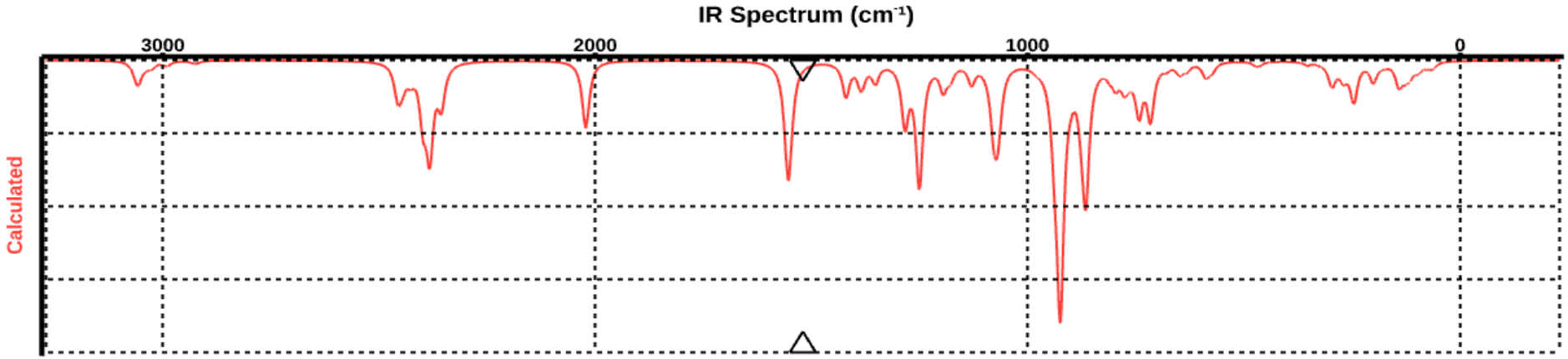

Figure S5. Calculated (ωB97X-D/6-316*/LANL2Dζ) Infrared Spectrum of $[Rh_2(\mu\text{-}CC_6H_4)HCl_2(\mu\text{-}dHpm)_2]$.

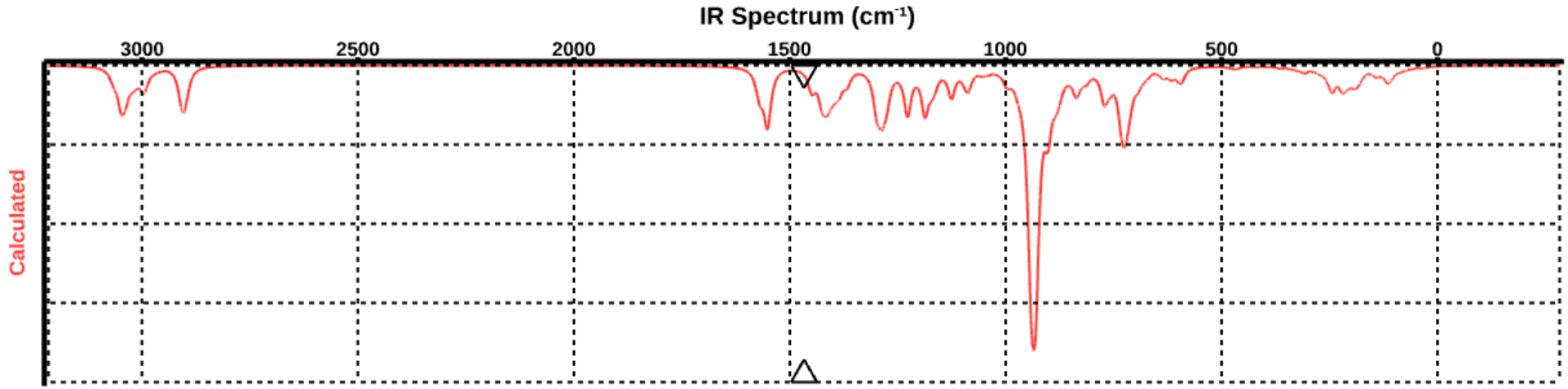

Figure S6. Calculated (ωB97X-D/6-316*/LANL2Dζ) Infrared Spectrum of $[Rh_2(\mu\text{-}CC_6H_4)(C_6H_5)Cl_2(\mu\text{-}dmpm)_2]$.

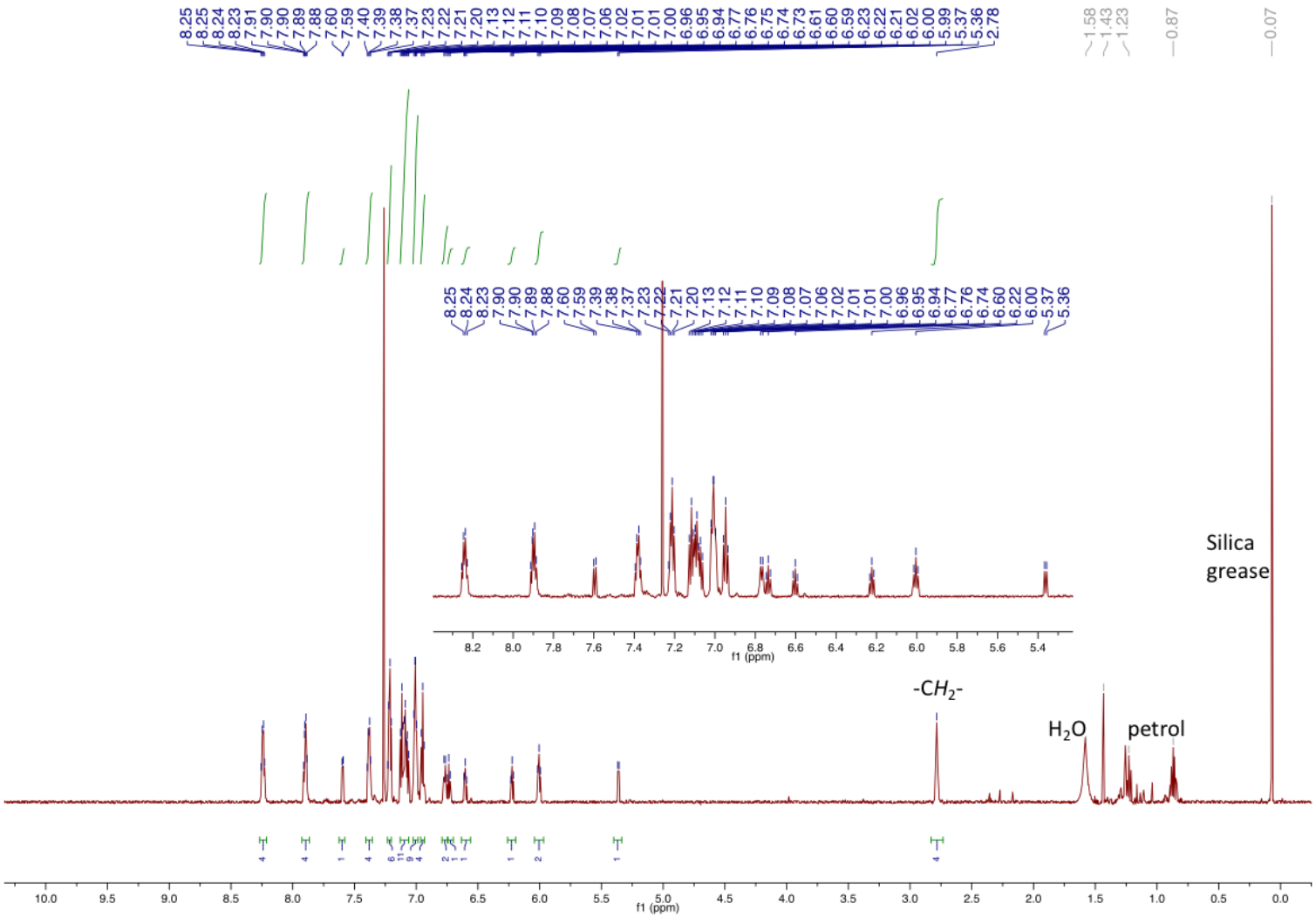

Figure S7. ^{1}H NMR (400 MHz, $CDCl_3$, 298 K, δ) of $[Rh_2(\mu\text{-}^{13}CC_6H_4)(\mu\text{-}Cl)(C_6H_5)Cl_2(\mu\text{-}dppm)_2]$ (2).

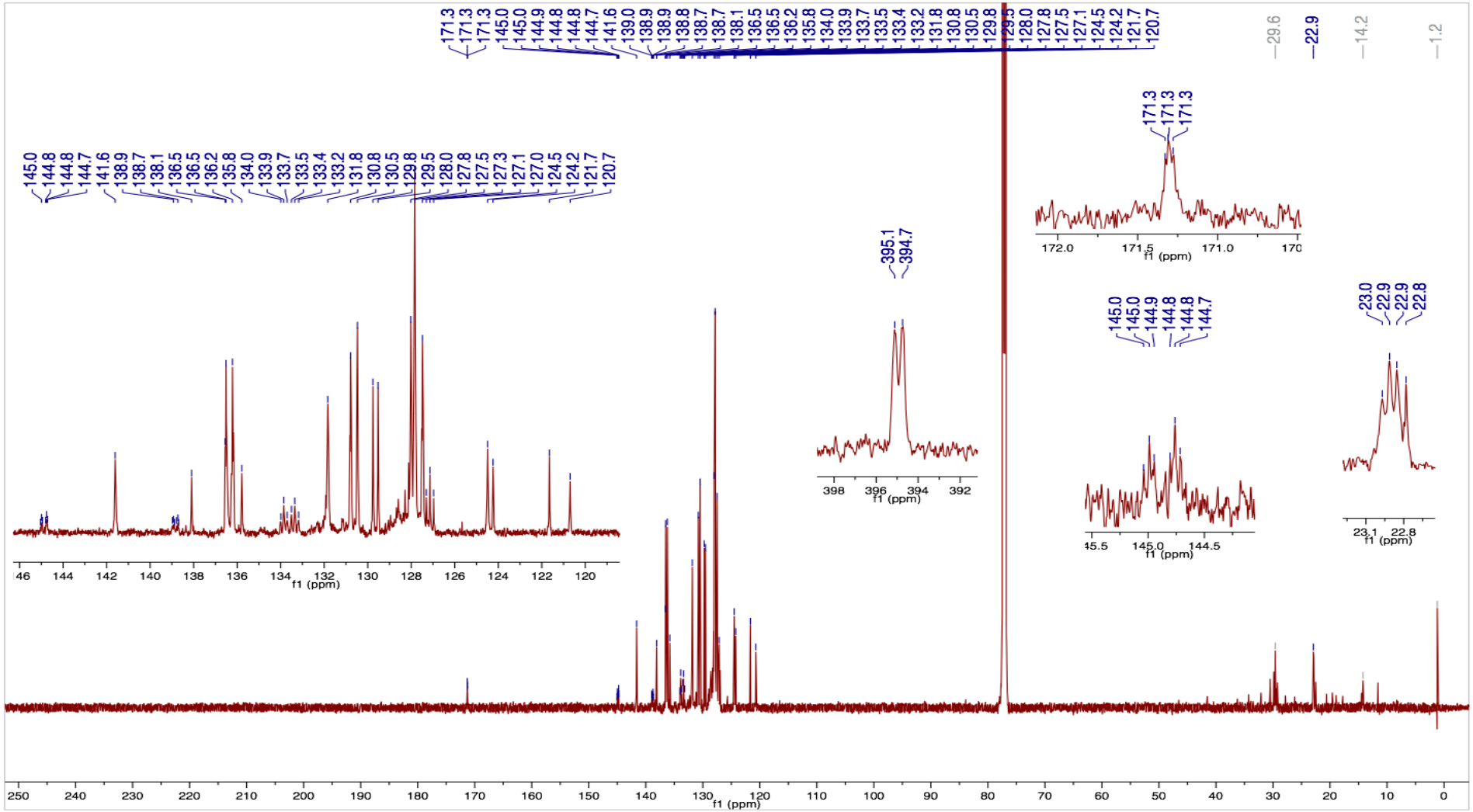

Figure S8. $^{13}C\{^{1}H\}$ NMR (151 MHz, $CDCl_3$, 298 K, δ) of $[Rh_2(\mu\text{-}^{13}CC_6H_4)(\mu\text{-}Cl)(C_6H_5)Cl_2(\mu\text{-}dppm)_2]$ (2).

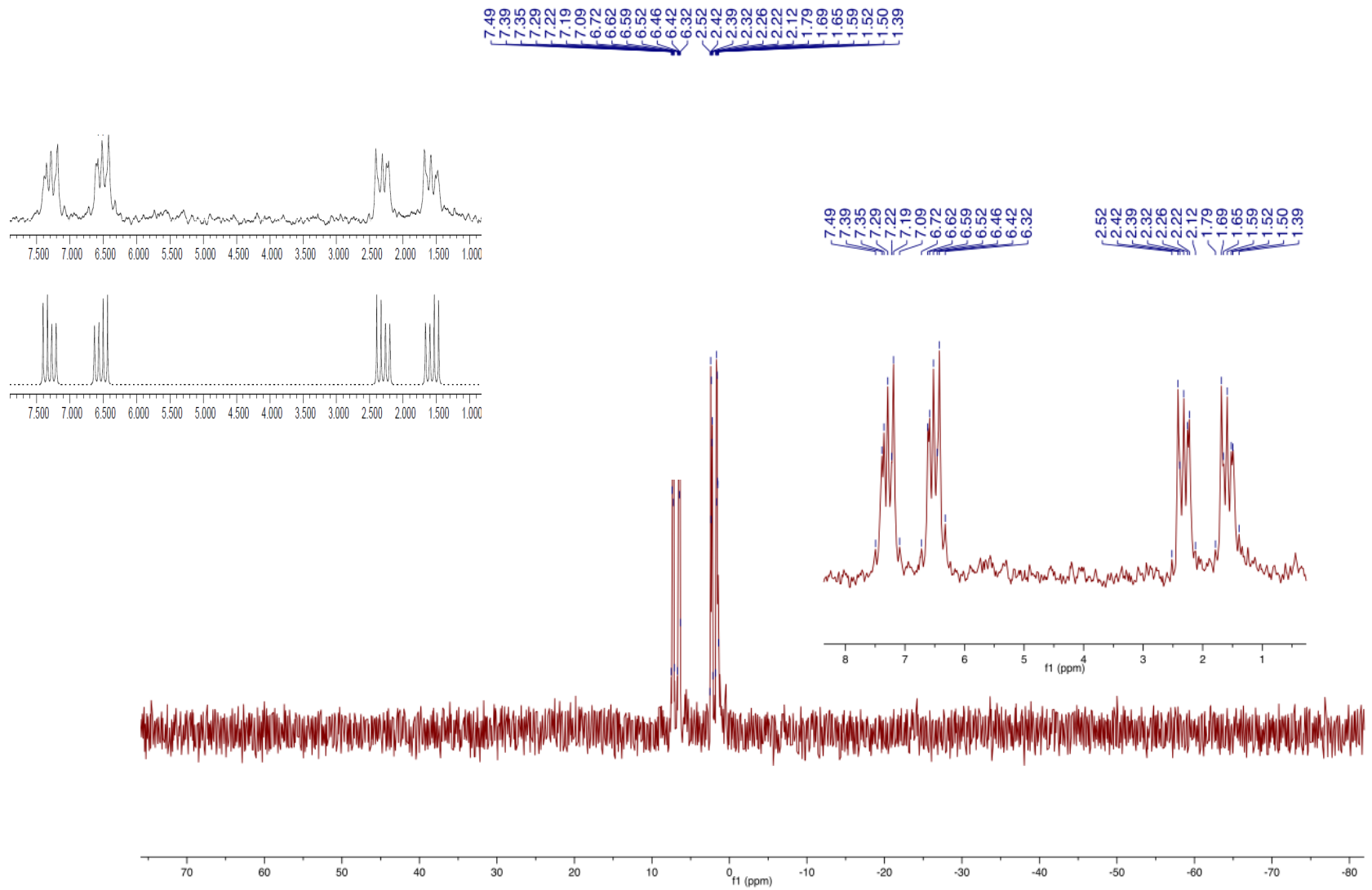

Figure S9. $^{31}P\{^{1}H\}$ NMR (162 MHz, $CDCl_3$, 298 K, δ) of $[Rh_2(\mu\text{-}^{13}CC_6H_4)(\mu\text{-}Cl)(C_6H_5)Cl_2(\mu\text{-}dppm)_2]$ (2) (left inset – simulated spin system developed using gNMR).

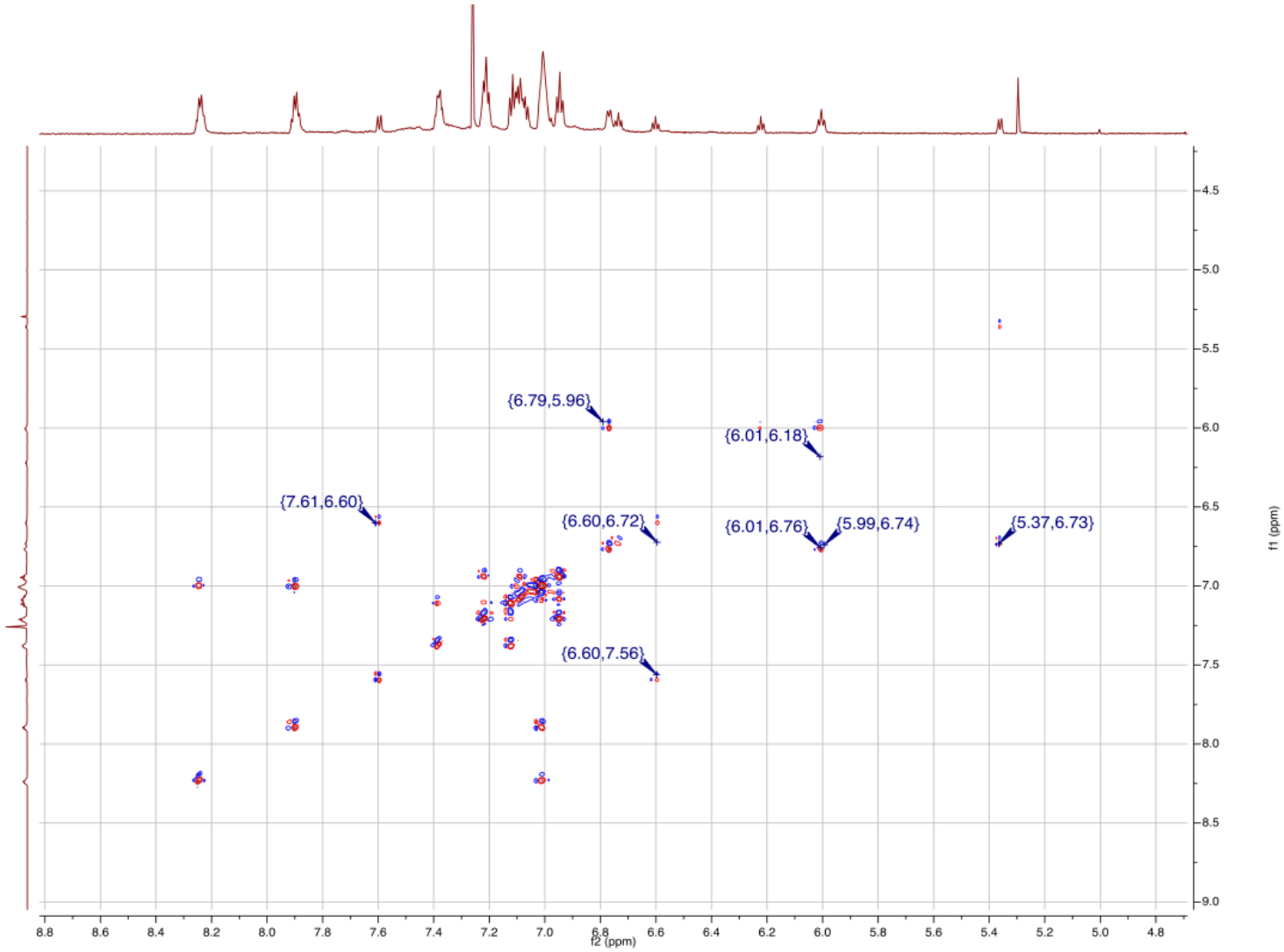

Figure S10. ^{1}H-^{1}H COSY NMR Spectrum (600 MHz, $CDCl_3$, 298 K, δ) of $[Rh_2(\mu\text{-}CC_6H_4)(\mu\text{-}Cl)(C_6H_5)Cl_2(\mu\text{-}dppm)_2]$ (2).

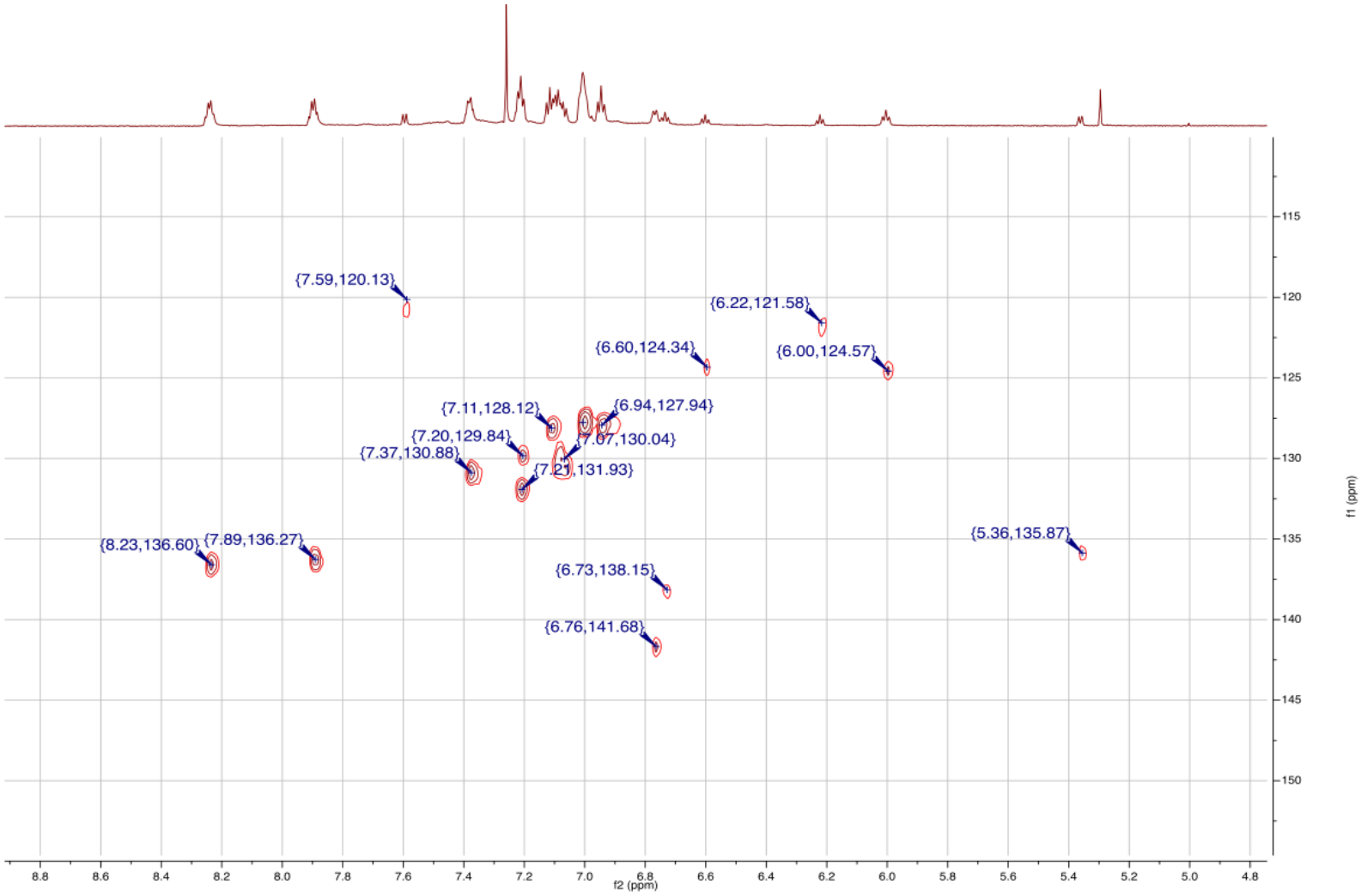

Figure S11. ^{1}H-^{13}C HSQC NMR (600 MHz, $CDCl_3$, 298 K, δ) of $[Rh_2(\mu\text{-}CC_6H_4)(\mu\text{-}Cl)(C_6H_5)Cl_2(\mu\text{-}dppm)_2]$ (2).

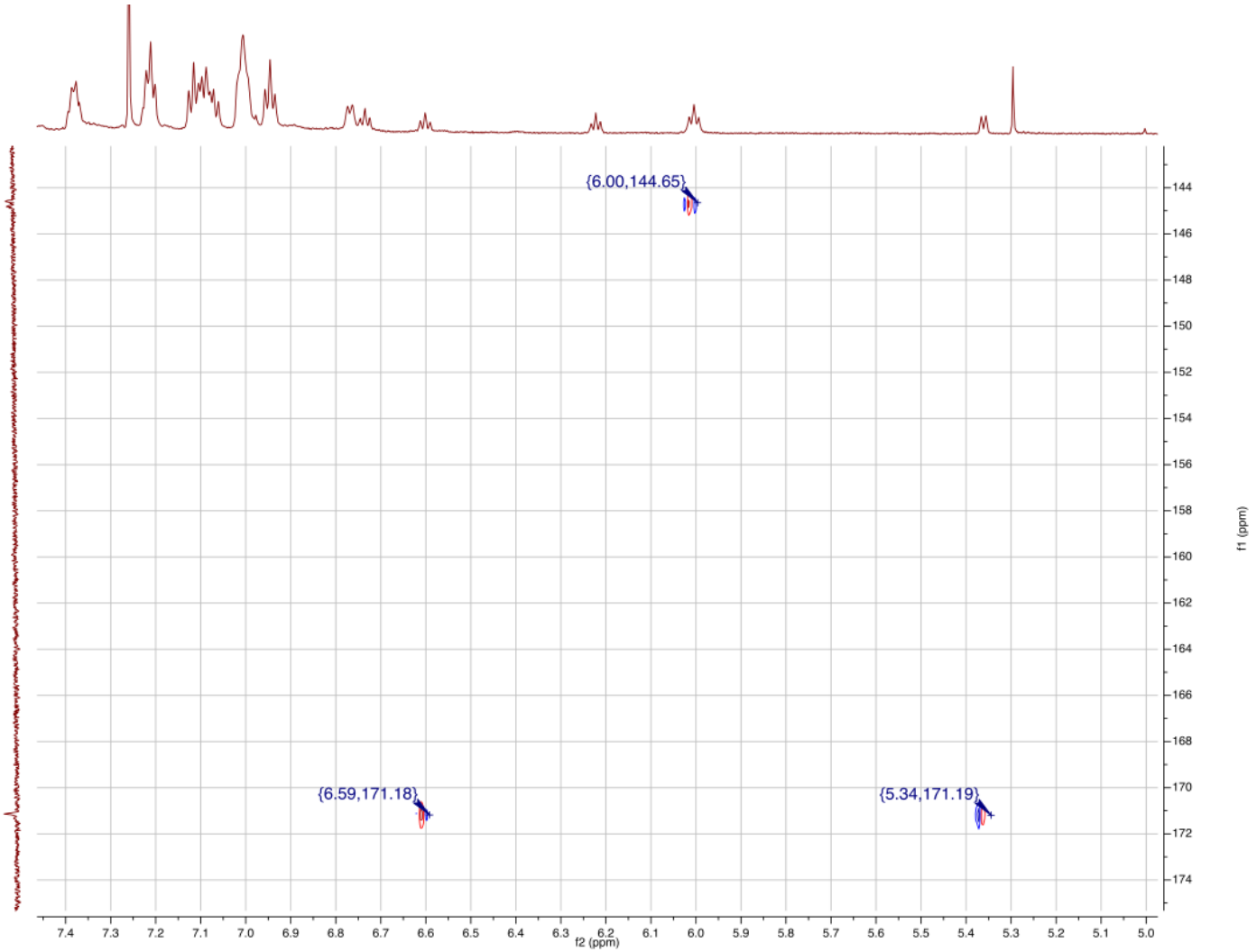

Figure S12. ^{1}H-^{13}C HMBC NMR Extract (600 MHz, $CDCl_3$, 298 K, δ) of $[Rh_2(\mu\text{-}^{13}CC_6H_4)(\mu\text{-}Cl)(C_6H_5)Cl_2(\mu\text{-}dppm)_2]$ (2).

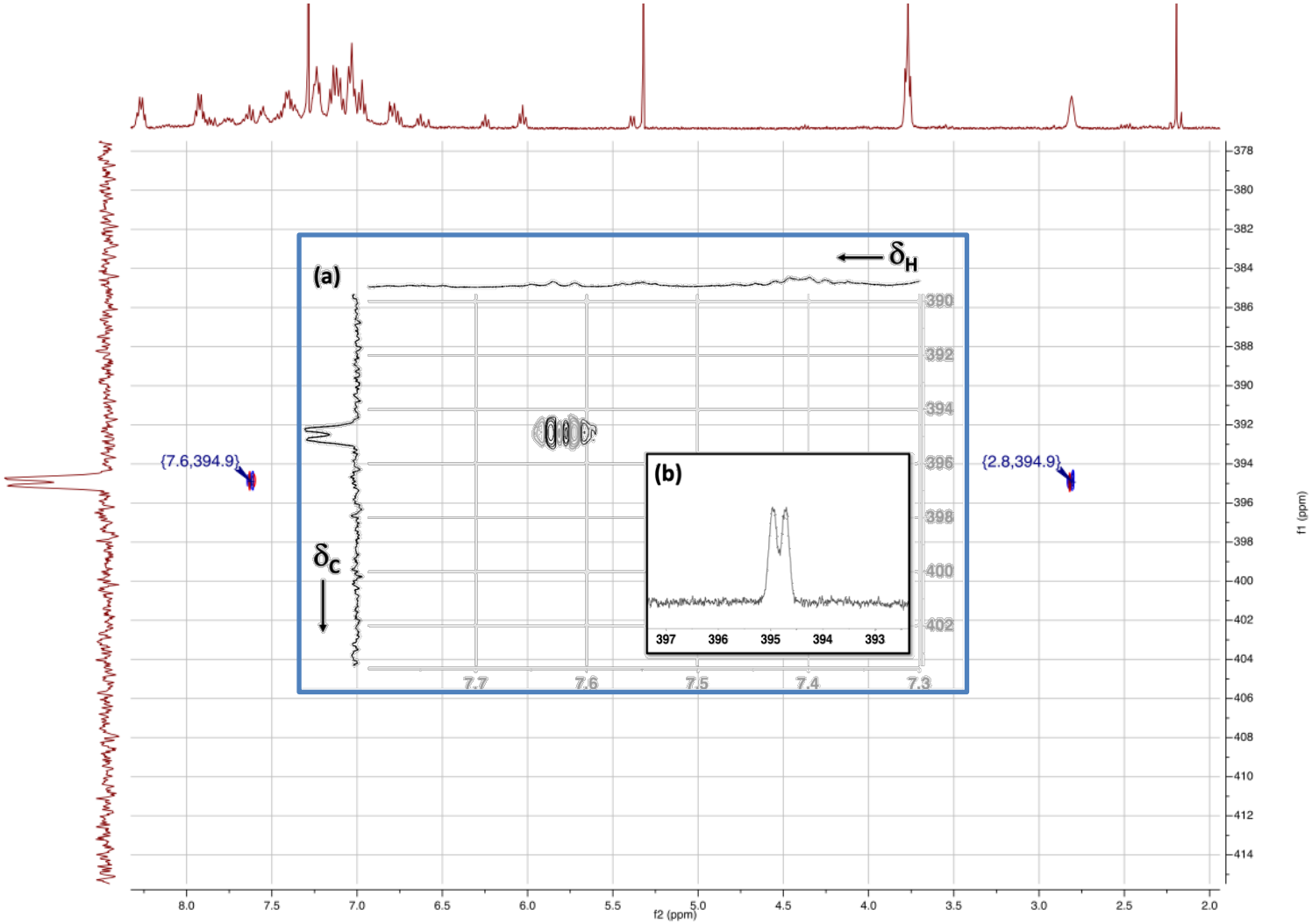

Figure S13. ^{1}H-^{13}C HMBC NMR Extract (600 M Hz, $CDCl_3$, 298 K, δ) of $[Rh_2(\mu\text{-}^{13}CC_6H_4)(\mu\text{-}Cl)(C_6H_5)Cl_2(\mu\text{-}dppm)_2]$ (2) - 50% 13C enriched at μ-C.

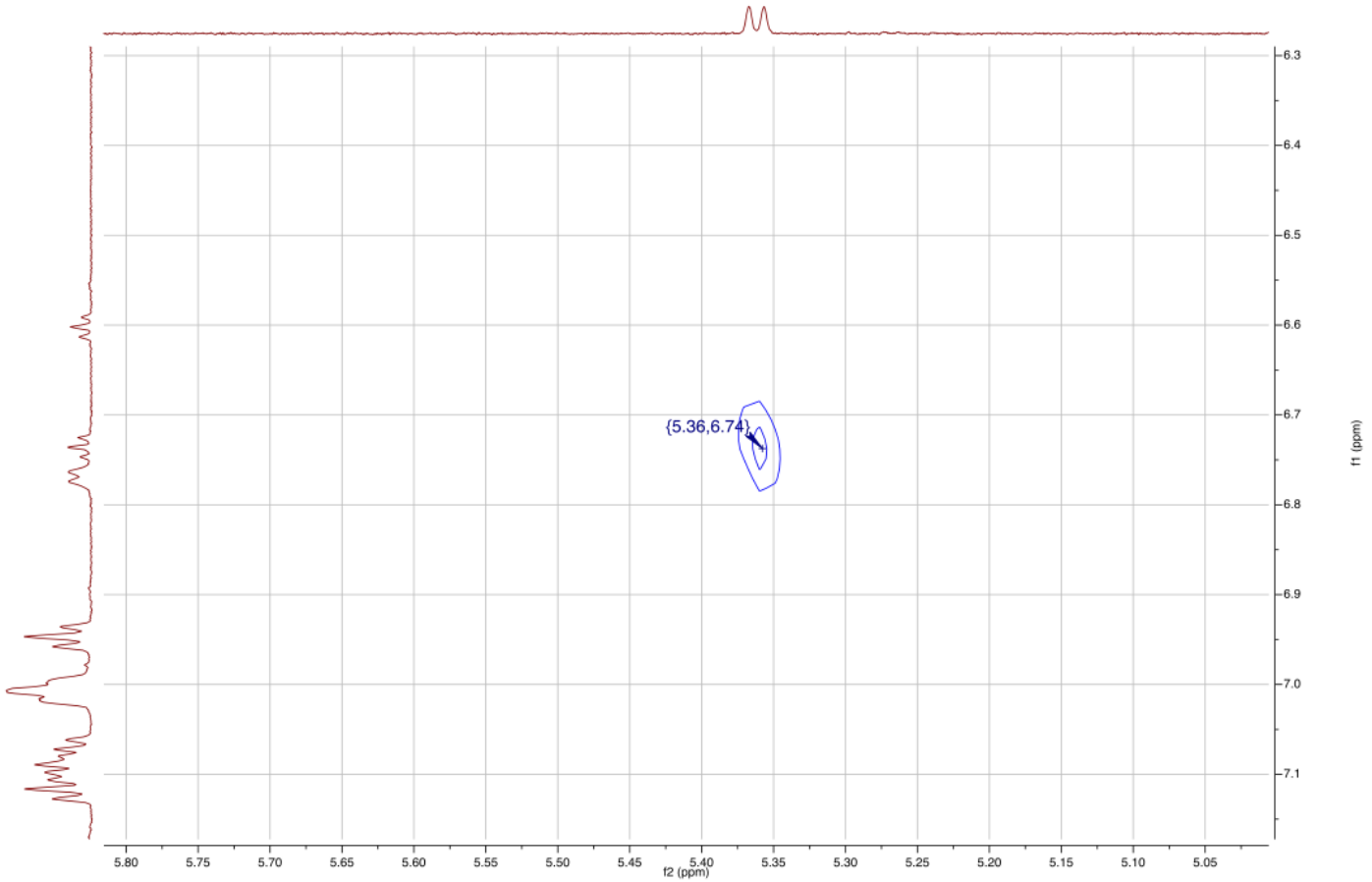

Figure S14. ^{1}H-^{1}H ROESY NMR Extract (600 MHz, $CDCl_3$, 298 K, δ) of $[Rh_2(\mu\text{-}CC_6H_4)(\mu\text{-}Cl)(C_6H_5)Cl_2(\mu\text{-}dppm)_2]$ (2).

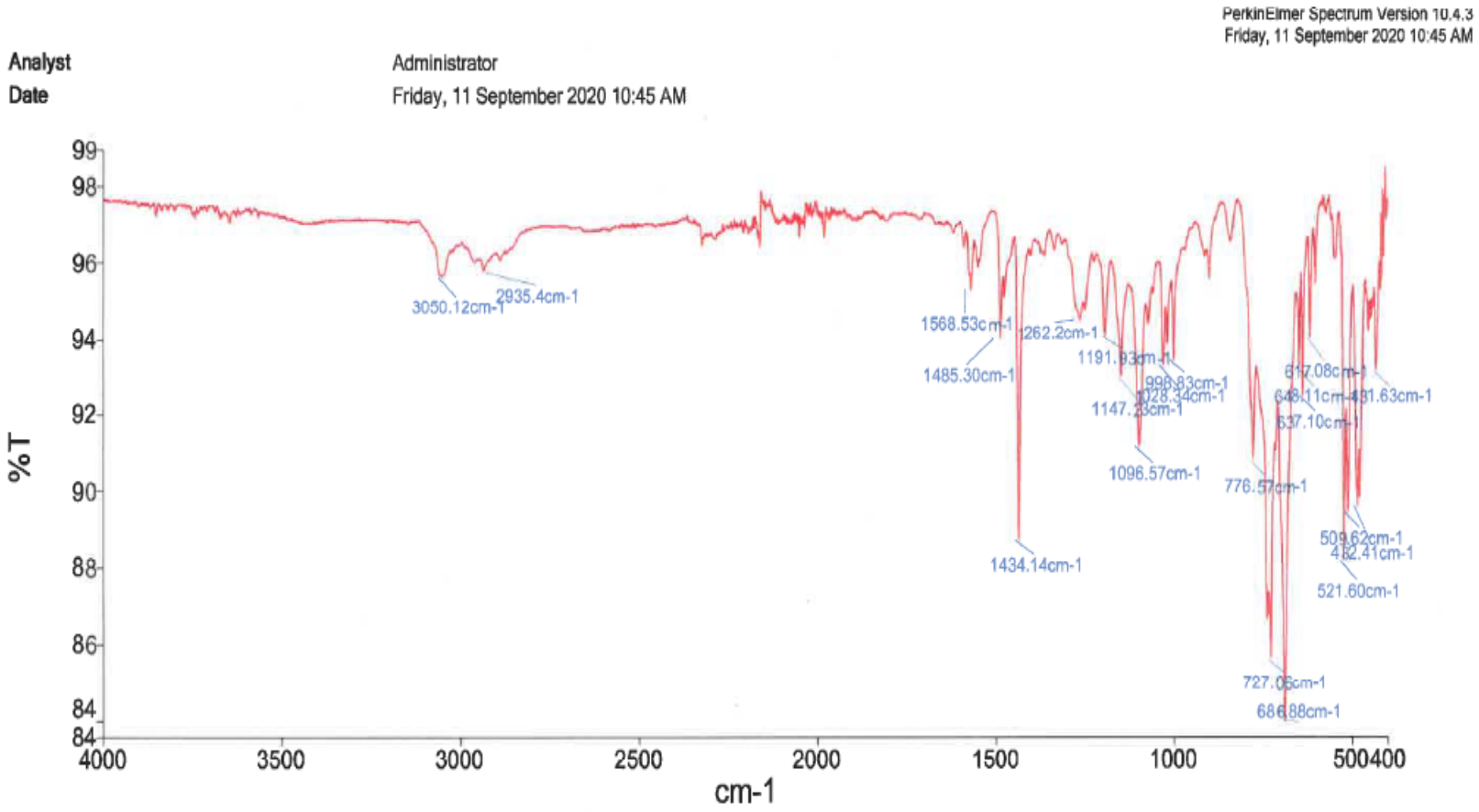

Figure S15. ATR IR Spectrum of $[Rh_2(\mu\text{-}CC_6H_4)(\mu\text{-}Cl)(C_6H_5)Cl_2(\mu\text{-}dppm)_2]$ (2).

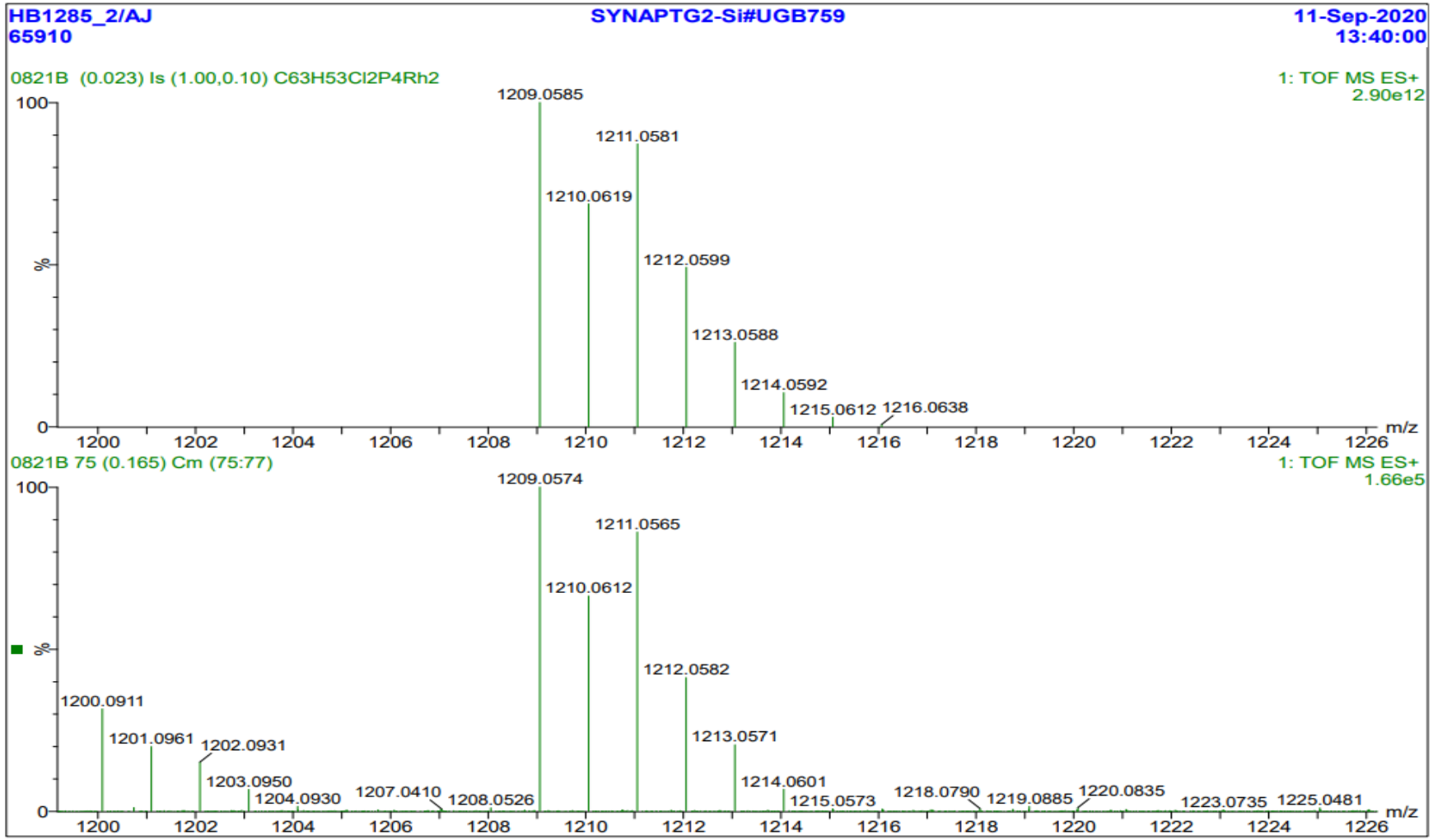

Figure S16. ESI-MS isotopic distribution and model of $[Rh_2(\mu\text{-}CC_6H_4)(\mu\text{-}Cl)(C_6H_5)Cl_2(\mu\text{-}dppm)_2]$ (2). $[M\text{-}Cl]^+$

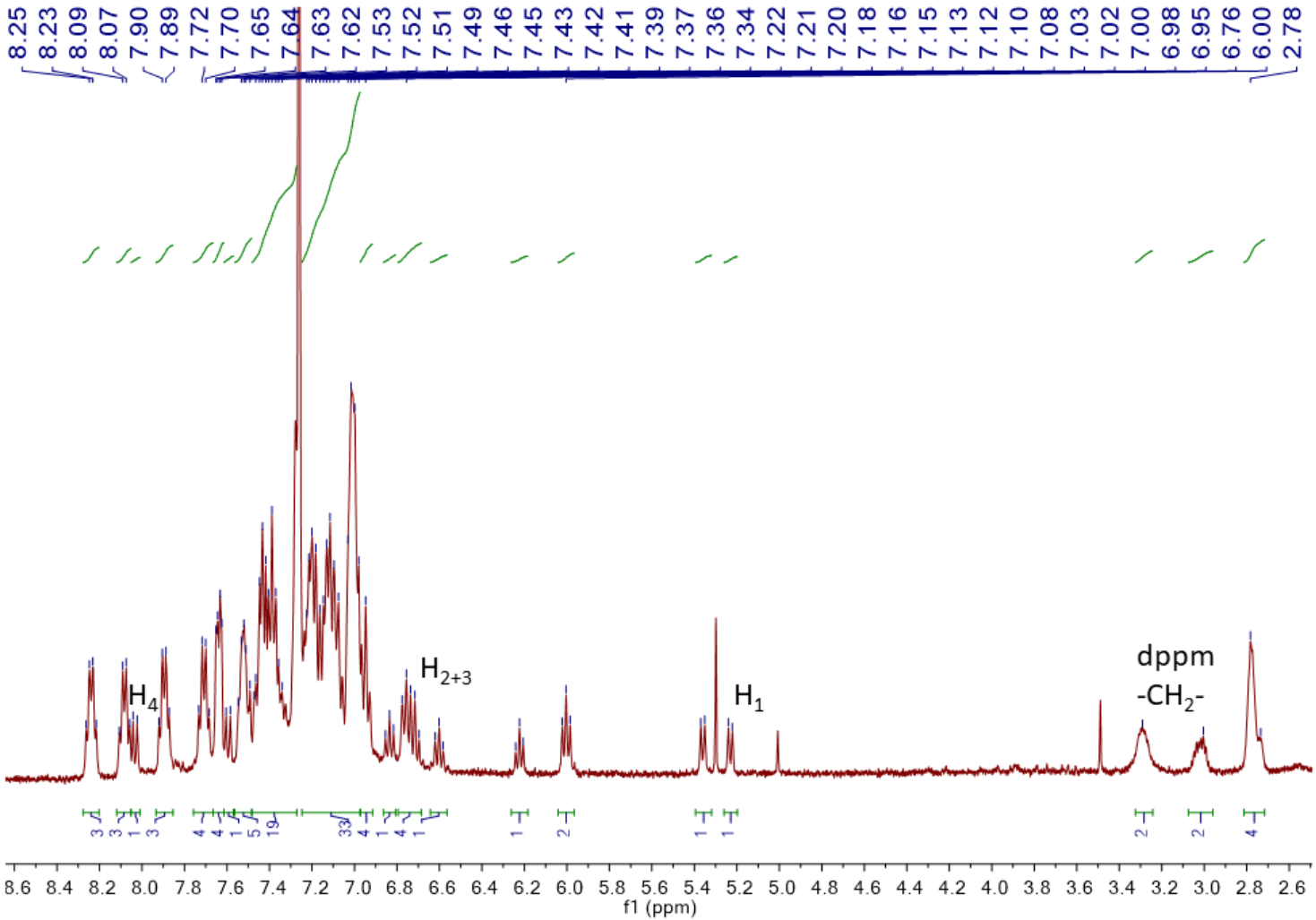

Figure S17. ^{1}H NMR (400 MHz, $CDCl_3$, 298 K, δ) inset of $[Rh_2(\mu\text{-}CC_6H_4)(\mu\text{-}Cl)(R)Cl_2(\mu\text{-}dppm)_2]$ (R = C_6H_5 2, Cl 4).

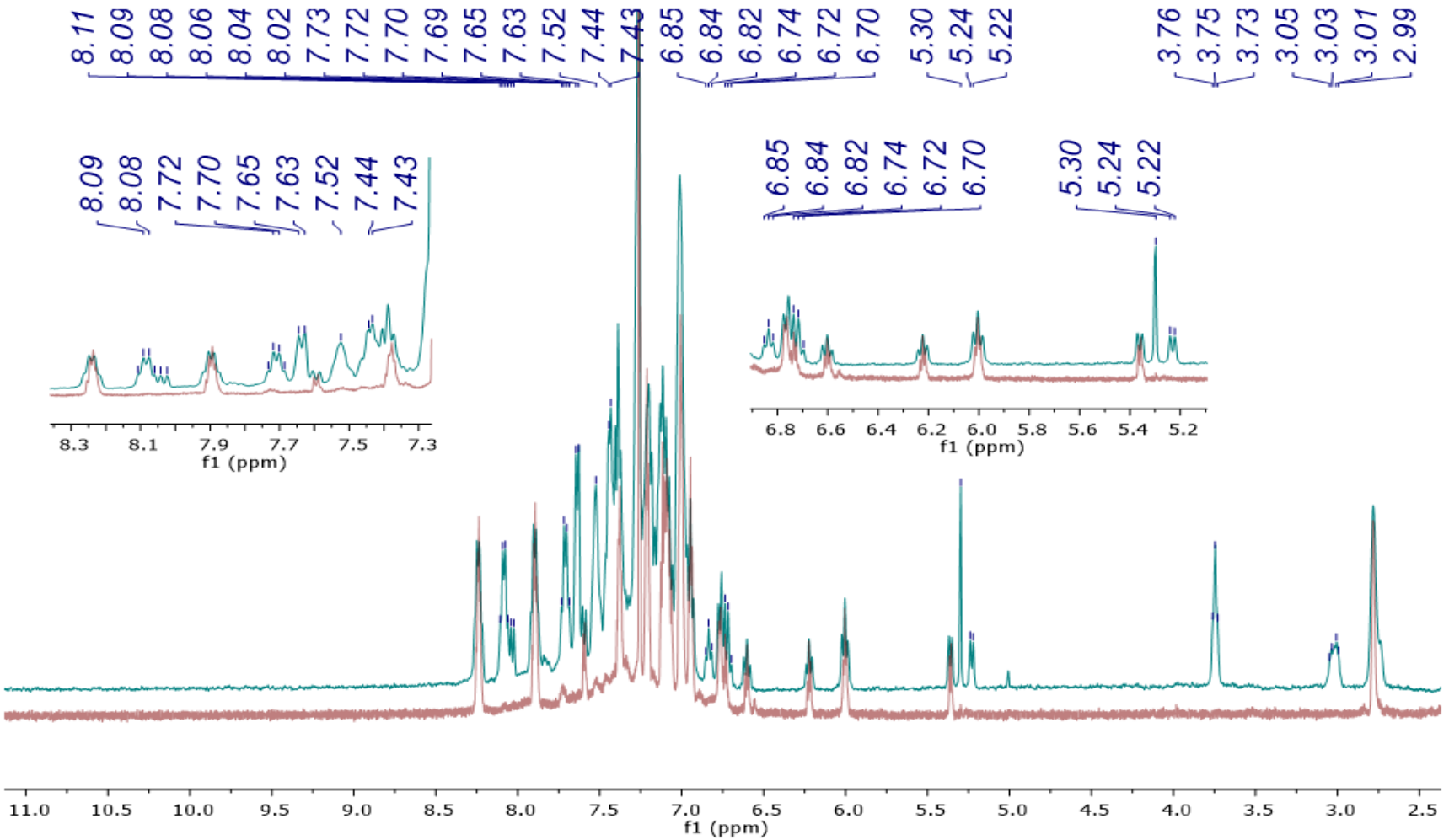

Figure S18. ^{1}H NMR (400 MHz, $CDCl_3$, 298 K, δ) extract overlay of $[Rh_2(\mu\text{-}CC_6H_4)(\mu\text{-}Cl)(R)Cl_2(\mu\text{-}dppm)_2]$ (R = C_6H_5 2, Cl 4, cyan) with 2 (red).

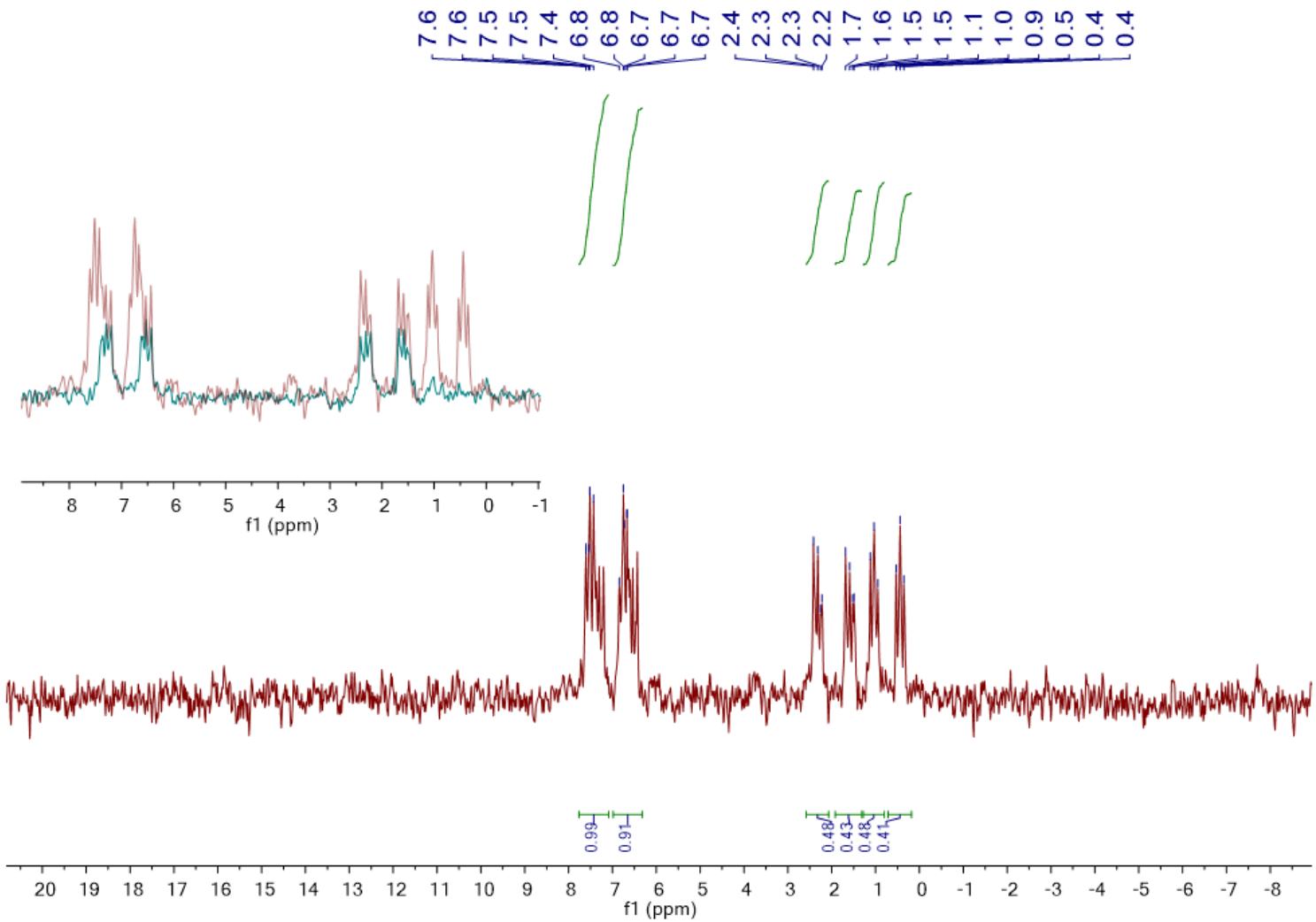

Figure S19. $^{31}P\{^{1}H\}$ NMR (162 MHz, $CDCl_3$, 298 K, δ) of $[Rh_2(\mu\text{-}CC_6H_4)(\mu\text{-}Cl)(R)Cl_2(\mu\text{-}dppm)_2]$ (R = C_6H_5 **2**, Cl **4**). Inset: overlay (red) with **2** (cyan).

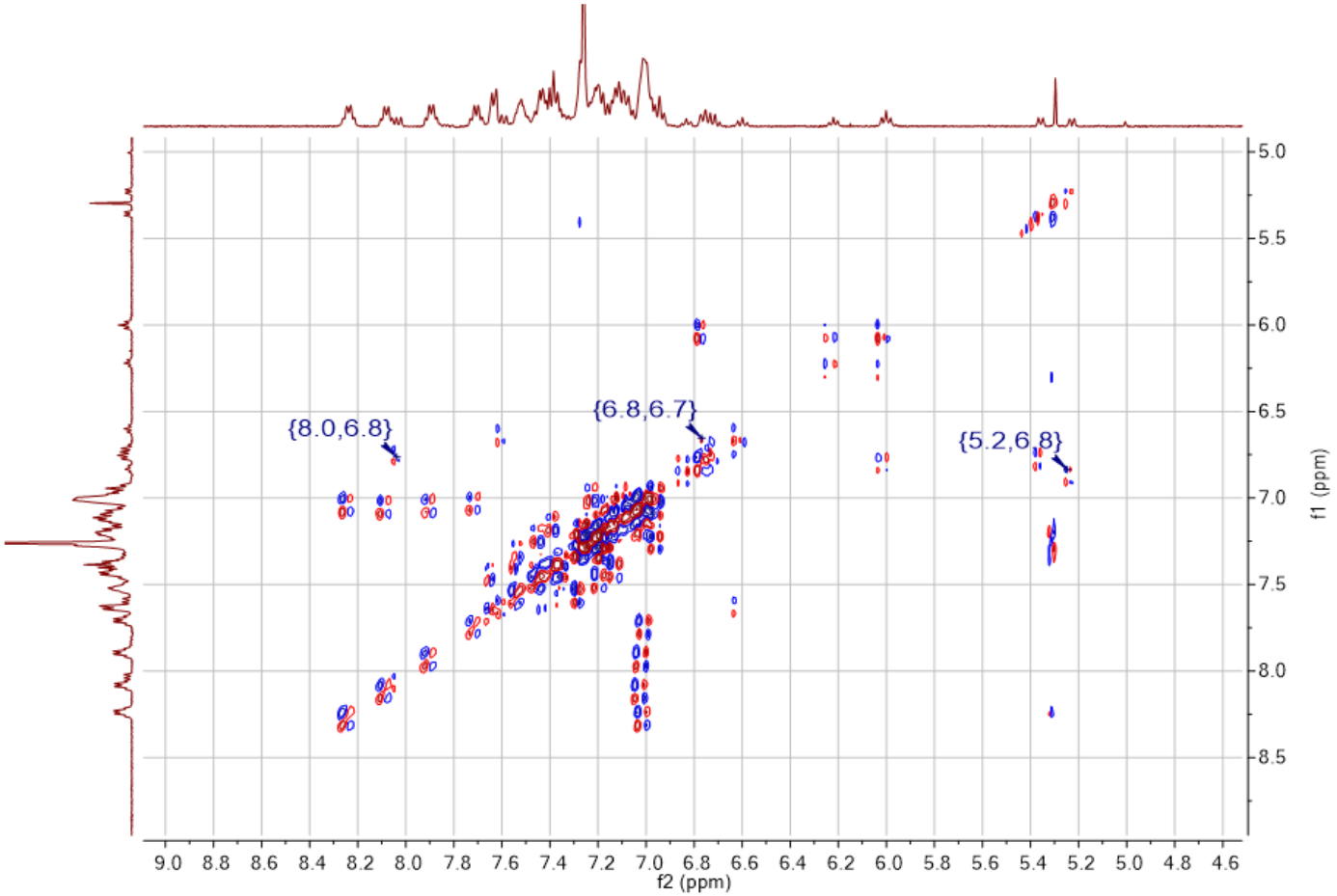

Figure S20. ^{1}H-^{1}H COSY NMR (400 MHz, $CDCl_3$, 298 K, δ) extract of $[Rh_2(\mu\text{-}CC_6H_4)(\mu\text{-}Cl)(R)Cl_2(\mu\text{-}dppm)_2]$ (R = C_6H_5 2, Cl 4).

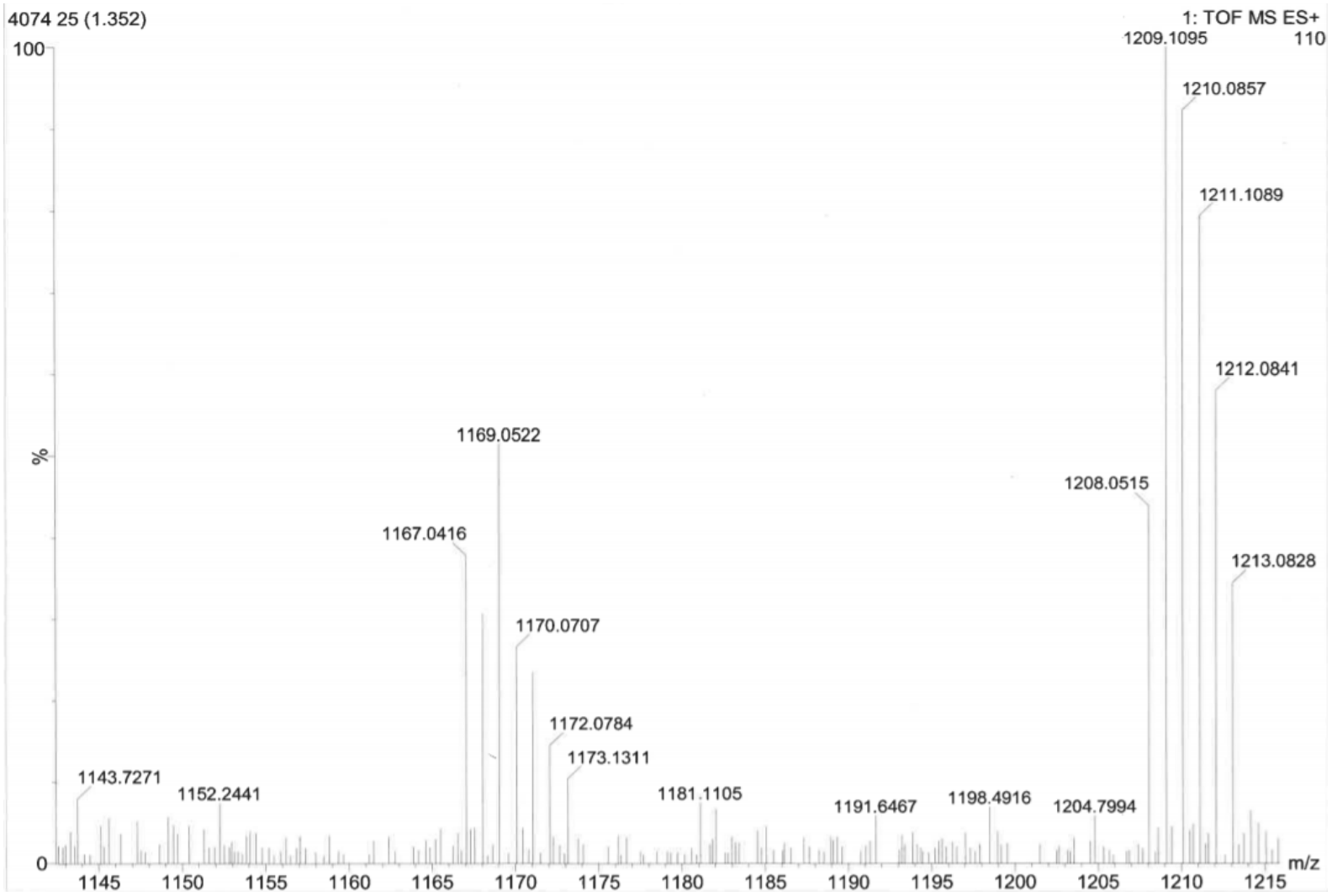

Figure S21. ESI-MS $[M\text{-}Cl]^+$ fragmentations of $[Rh_2(\mu\text{-}CC_6H_4)(\mu\text{-}Cl)(R)Cl_2(\mu\text{-}dppm)_2]$ (R = C_6H_5 **2**, Cl **4**).

Dalton Transactions